A bilateral symmetry based pose normalization framework applied to livestock body measurement in point clouds

Article *in* Computers and Electronics in Agriculture · March 2019

DOI: 10.1016/j.compag.2019.03.010

CITATIONS
19

READS
525

7 authors, including:

Guo Hao
China Agricultural University
44 PUBLICATIONS **393** CITATIONS
SEE PROFILE

Wei Su
China Agricultural University
77 PUBLICATIONS **1,581** CITATIONS
SEE PROFILE

Francesco Marinello
University of Padova
206 PUBLICATIONS **2,821** CITATIONS
SEE PROFILE

Computers and Electronics in Agriculture

journal homepage: www.elsevier.com/locate/compag

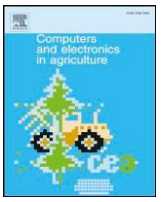

A bilateral symmetry based pose normalization framework applied to livestock body measurement in point clouds

Hao Guo[a,*], ZhenBo Li[b], Qin Ma[b], DeHai Zhu[a], Wei Su[a], Ke Wang[a], Francesco Marinello[c]

[a] College of Land Science and Technology, China Agricultural University, Beijing 100083, China
[b] College of Information and Electrical Engineering, China Agricultural University, Beijing 100083, China
[c] Department of Land, Environment, Agriculture and Forestry, University of Padova, Viale dell'Universitá 16, 35020 Legnaro (PD), Italy

ARTICLEINFO

Keywords:
Animal
Precision livestock farming
Dimension measurement
Livestock weighing
Automatic

ABSTRACT

The shape of a livestock is a vital indicator of its health and value, whether for breeding or growth. Cutting-edge remote sensing technology provides an efficient and affordable way for acquiring point clouds of livestock, so that automated procedures of obtaining body measurements need to be established. A novel pose normalization method for 3D point clouds of livestock with similar forms of cows or pigs based on its bilateral symmetry properties is proposed in order to increase the degree of measuring automation. The proposed algorithm is combined in a hybrid scheme, which serves as the pose normalization procedure in an automatic body measurement system for livestock. Our extensive experiments on both synthetic and real world point clouds data show that the proposed approach has potential for generalizing well across livestock species and handles noise successfully in test data. In addition, the proposed pose normalization scheme outperforms current standard approach Principal Component Analysis (*PCA*) and state-of-the-art pose normalization method for pigs.

1. Introduction

The shape of an animal is an essential signal for the expression of its health and value (Savin et al., 2011; Klingenberg, 2010). Body measurements have been the most straightforward way to quantify the shape of individual animal within the field of precision livestock farming. However, in addition to time consuming and costly for farmers (Azzaro et al., 2011), manual body measurement can induce high levels of stress to the animals (Tasdemir et al., 2011).

To overcome the limitations of conventional measurement system, machine vision has been used extensively as a non-intrusive approach for animal body measurement (Kuzuhara et al., 2015). Several researchers assessed the feasibility of utilizing video and digital images to determine body shape in dairy cows (Tasdemir et al., 2011; Azzaro et al., 2011), pigs (Brandl and Jorgensen, 1996, 1999, 2015), sheep (Yilmaz et al., 2013; Menesatti et al., 2014), and horse (Pallottino et al., 2015). However, the use of 2D image technology in livestock related settings and barn environments comes with several technical challenges, e.g., diffuse light conditions, unpredictable animal movements and limiting applications utilizing 3D body measurements due to the lack of the third dimension (Salau et al., 2017; Mortensen et al., 2016). Stereo vision techniques have been introduced to monitor pigs in three dimensions. Schofield et al. have shown that a 3D stereo imaging system successfully captured the 3D shape and visual appearance of live pigs (Wu et al., 2004). But this system need that pigs to stand properly in the corner of a large pen for the purposes of imaging. These stereo vision systems are also difficult to use in practice, due to the difficulty of homologous point matching in farming conditions. Novel remote sensing technology, e.g., depth sensors offer great potential for measurement applications (Lichti et al., 2012), which can handle the problems caused by conventional 2D image systems, and stereo vision techniques. Over the past few years, there has been a dramatic increase in the use of range cameras in livestock farming (Weber et al., 2014; Pezzuolo et al., 2018; Song et al., 2018). Recently, consumer depth cameras based on structured infrared-light(IR) system, such as Kinect or Xtion Pro, provide point clouds at a low cost and have opened tremendous new opportunities for capturing the geometry of livestock (Salau et al., 2017; Kawasue et al., 2013; Viazzi et al., 2014; Mortensen et al., 2016; Guo et al., 2017; Pezzuolo et al., 2018; Pezzuolo et al., 2018; Song et al., 2018). Weber et al. has developed the system for recording 3D images, taken many cuts along aligned cow's surface so as to determine traits that are relative to the surface's deformation induced by varying body condition (Weber et al., 2014). However it is worth mentioning that they only observed the back of body surface of cow. A 3D scanning system for live cattle using multiple Kinect was established, where the key traits for evaluating the conformation of cow

* Corresponding author.
E-mail address: guohaolys@cau.edu.cn (H. Guo).

https://doi.org/10.1016/j.compag.2019.03.010
Received 18 October 2018; Accepted 9 March 2019

were estimated by using point clouds aligned with tilt sensor (Kawasue et al., 2013). Furthermore they introduced one black cattle body shape and temperature measurement system recently (Kawasue and Khin, 2017). The feasibility for using back posture measurements of cows with 3D sensor to predict body weight and milking traits was evaluated (Kuzuhara et al., 2015). The contribution of this research is that they introduce geodesic distance on particular body regions in order to obtain body condition score. Salau et al. implemented a 3D reconstruction system comprising six depth cameras for monitoring purposes in dairy cows(Salau et al., 2016) and extracted measurements of udder and rear legs of cows from the point clouds of cows automatically (Salau et al., 2017). However, available literature is lacking with regard to the metrological performance. Therefore Pezzuolo et al. discussed metrological implementation of a low cost 3D depth camera technology to allow for extraction of quantitative cow body parameters (Pezzuolo et al., 2018).

Based on above, we may safely conclude that many of the current systems were designed only for part of specific livestock body, and they also avoid or ignore the fundamental issue (pose normalization) before measurement by manually inputting reference points or using tilt sensor. The best-known approach for pose normalization is Principal Component Analysis (*PCA*) or Karhunen-Loeve transformation (Vranic et al., 2001). The *PCA* algorithm, based on the computation of 3D object moments, estimates the principal axes of a 3D object that are used to determine its orientation. In its original form, *PCA* has a number of disadvantages: it can be imprecise and often the principal axes of 3D objects that belong to the same class produce poor alignments (Chen et al., 2003). To alleviate these problems, the Continuous Principal Component Analysis (*CPCA*) algorithm and the Normal Principal Component Analysis (*NPCA*) algorithm have been proposed to improve the original *PCA* method(Papadakis et al., 2007). The *PCA*-based pose normalization methods and especially the *CPCA* and *NPCA* variants, though general and well performing in most cases, can fail to capture some specific characteristics of 3D objects such as symmetries and large planar or bumpy surfaces. State of the art livestock pose normalization research shows that *PCA* based normalization method is heavily dependent on data. Data with non symmetric missing parts or with pigs's head aside would produce incorrect pose normalization results (Guo et al., 2017). Another major category of normalization methods exploits symmetry characteristics found in a large number of 3D objects (Bevilacqua et al., 2009; Sfikas et al., 2011; Sfikas et al., 2014). The last category of normalization methods employs application specific geometric information to get the accurate shape alignment (H.M. and R.D., 2016). For instance, ground plane normal vector was introduced in order to consistently align buildings (Zhang et al., 2013). While Farrugia et al. investigated the various pose normalization techniques that can be used for 3D vehicle models (Farrugia and Barbarar, 2015). However, most approaches are designed for application of face recognition and 3D objects retrieval purpose which do not need optimal alignment. Additionally, they can not define directions of axes consistently, leading to ambiguous errors in livestock body measurements. To efficiently extract measurements from data, it is necessary to be able to automatically segment out the livestock from the scene and align the corresponding point clouds in a predefined canonical coordinate system (*CCS*) (Sfikas et al., 2011). Over the past few decades, a large number of studies contributing to 3D point clouds processing have been investigated, most of these are devised for mapping, autonomous vehicle navigation, forest assessment, building information modeling and some industrial applications. However, it appears that far less attention has been devoted to the automatic processing of livestock point clouds for the field of precision livestock farming. To fulfill the gap, inspired by state-of-the-art pose normalization method based on 2d panoramic view (Sfikas et al., 2014), this paper propose a fully automatic 3D point clouds pose normalization framework in order to automatically process livestock point clouds. The main contributions of this paper are as follows:

- A fully automatic pose normalization framework is proposed by the combination of a novel symmetry detection and estimation of forward direction of livestock, outperforming standard approach *PCA* and state-of-the-art pose normalization method (Wang et al., 2017) for pigs.
- The proposed pose normalization pipeline is incorporated in an automatic point clouds processing system for livestock body measurement which generalizes well across livestock species, providing a novel solution for precision livestock farming (PLF).
- An updated 3D point clouds processing software for livestock shape analysis can be downloaded freely from (Hao, 2017) to livestock industry and research community.

2. Materials and methods

2.1. 3D point clouds requirements

In order to design the algorithms, it is important to make some assumptions about the input 3D data for new proposed method. We apply assumptions made in paper (Guo et al., 2017) to input point clouds of this study. Specifically, let's begin with a point cloud denoted by $S = \{p_i\}$. We assume that S are composed of one animal standing on flat ground both with and without possible parts of other farm facilities. In addition, we require that the livestock to be monitored have similar forms of cows or pigs, that is to say that a livestock has large body in relation to their head size, shorter hair (it actually depends on breed when we're considering real applications), and so on. For more details of assumptions about the input 3D data, please refer to paper (Guo et al., 2017). Fig. 1 shows one qualified input data acquired by using one prototype system for animal 3D scanning (Guo et al., 2017). In order to guarantee that point clouds data acquired comply with the assumption, we kept other livestock away from the one to be monitored in practice.

2.2. SPECIFICATION of pose NORMALIZATION ALGORITHM

The aim of pose normalization is to align the livestock with the *CCS* through a rigid 3D transformation. Therefore, the *CCS* must be defined precisely (see Section 2.2.1). The proposed processing pipeline for pose normalization is shown in Fig. 2. The first step deals with detection of the ground plane and segmentation of livestock. Starting from the point clouds of livestock segmented and the normal vector of ground plane detected, its bilateral symmetry plane is estimated by using a novel voting scheme. We, then, use application-specific geometric feature to identify the forward direction of livestock and compute the three axes of *CCS*. Additionally, a 3D rigid alignment is estimated to be used for performing pose normalization of the livestock. Sections 2.2.2, 2.2.3, 2.2.4 and 2.2.5 provide more details on each step illustrated on a pose normalization example of Fig. 1.

Fig. 1. One example of qualified input point clouds.

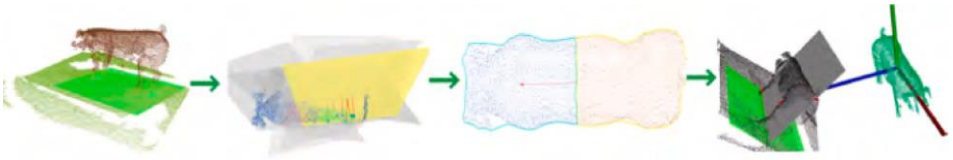

(a) Detection of ground plane and segmentation of livestock. (b) Bilateral symmetry plane estimation. (c) Forward direction estimation. (d) Pose normalization based on rigid transformation.

Fig. 2. A visual diagram of the proposed processing pipeline for pose normalization.

2.2.1. Canonical coordinate system definition for livestock

3D scanning of animals are usually given in arbitrary orientation and position in three dimension space. However, many traits are measured along the anterior-posterior axis or its dorsal-ventral axis when examining a livestock's conformation. Although it is not necessarily required for all automated measurement systems of 3D geometric shapes to employ pose normalization, however for many advanced methods, pose normalization (also known as alignment) is a critical procedure in their pipeline, so that the landmarks extraction algorithms which follow, are able to achieve a match between the (spatial) characteristics of the 3D objects (Sfikas et al., 2011). Hence, for the purpose of automated analysis of 3D livestock it is crucial to define an applicable canonical coordinate system. Considering facts that many traits are measured along anterior-posterior axis or dorsal-ventral axis, we define anterior-posterior axis and dorsal-ventral axis as two of the principal axes of the livestock. As seen from Fig. 3, the *CCS* for livestock uses the following axis definitions:

- The origin of *CCS* is positioned at the centroids of livestock.
- The positive Z-axis goes from the centroids of livestock to the right and is perpendicular to the symmetric plane of the livestock.
- The Y-axis is positive in the up direction, perpendicular to the ground plane.
- The positive X-axis goes from the centroids of livestock to the front and is determined by right-hand rule.

2.2.2. Detection of ground plane and segmentation of livestock

Based on the definition of Y-axis in the previous section. Once the ground plane is estimated, the Y-axis of the livestock is also defined as the normal to the ground plane if it points in the up direction of livestock. Therefore we start from downsampling point clouds S by using octree with leaf size d_r. All subsequent procedures are applied on donwsampled point clouds denoted by $D = \{p_i\}$. Then we apply RANdom SAmple Consensus (RANSAC) (Schnabel et al., 2007) to extract ground plane denoted by P_g . Here we describe the plane P_g by an equation of the vector form, known as the Hesse normal form. This form is:

$$\mathbf{n_g} \cdot \mathbf{r} - D_0 = \mathbf{0},$$

where $\mathbf{n_g}$ is a unit normal vector to the plane, is a position vector of a point of the plane and D_0 is the distance of the plane from the origin. Prior to further processing the segmentation of input point clouds into animal and background is a necessary task in our workflow. This livestock segmentation can be performed using algorithm proposed in (Guo et al., 2017). For more details on livestock segmentation we refer to (Guo et al., 2017). Let C^* denote the cluster of livestock segmented. Fig. 4 shows a visualization of livestock segmentation results on the data of Fig. 1.

In general, there is no mathematical way to make sure that the normal vector of ground plane points in the up direction of livestock. Because the orientation of the normal vector of ground plane depends on the order of points chosen for constructing the candidate plane at each iteration of RANSAC. For more details we refer to (Guo et al., 2017). To orient the normal of ground plane $\mathbf{n_g}$ consistently towards up direction of livestock, we take advantage of the fact that there are no livestock located under ground plane. Thus, we reverse the direction of the vector $\mathbf{n_g}$ under condition: $\mathbf{n_g}$ points in direction of ground plane sufficiently. The condition is implemented by testing whether $\mathbf{n_g} \cdot (\mathbf{O_g} - \mathbf{O_p}) \leqslant \mathbf{0}$, where $\mathbf{O_g}$ is the geometric center of ground plane P_g, $\mathbf{O_p}$ is the geometric center of livestock C^*. Fig. 4 shows a visualization of ground plane detected results on data from Fig. 1 and its corresponding normal vector $\mathbf{n_g}$ that is passed to the Section 2.2.5.

2.2.3. Bilateral symmetry plane detection of livestock

Symmetry is an essential and ubiquitous concept in the field of nature, science, and art. Bilateral symmetry is almost universal among animals. To utilize this observation, symmetric plane of livestock is employed to obtain the Z-axis of CCS. To do so, motivated by perpendicularity between symmetry plane of livestock and ground plane, we

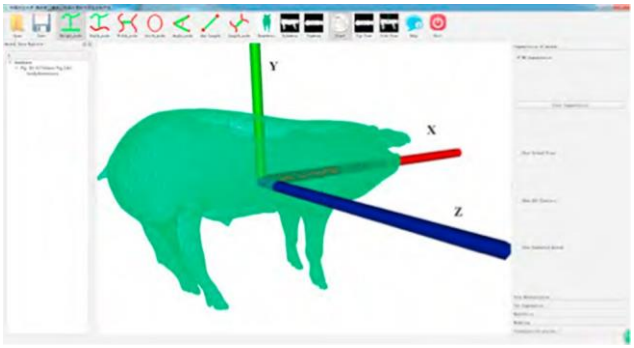

Fig. 3. The canonical coordinate system definition.

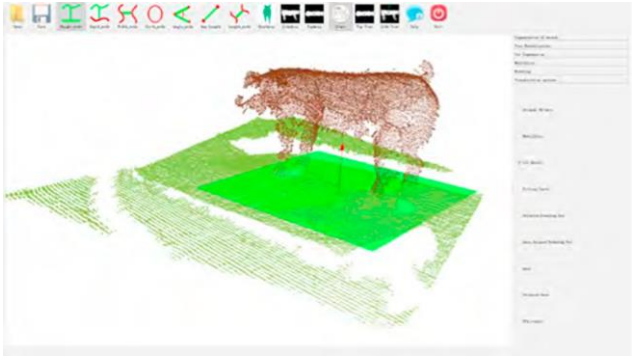

Fig. 4. Livestock segmentation results on the data of Fig. 1 and corresponding normal vector $\mathbf{n_g}$ of ground plane estimated.

separate the symmetry estimation into two phases: In the first step, we prune away a set of points on the 3D shape C_*. In the second step we choose a set of one-to-many samples on the pruned point clouds, apply the global symmetric transformations induced by these samples, and estimate bilateral symmetry plane based on the majority of votes. While sharing some similarities, our method is fundamentally different from global pairing-voting scheme (Mitra et al., 2006). We avoid the costly exhaustive search of the former by using pairing-voting scheme only AFTER we dramatically decrease the number of all potential symmetric mappings in each stage of our method. The following paragraphs will elaborate on the individual steps and provide more details.

Point pruning. In the first stage, our goal is to find part of 3D shape C_* obtained from last section that are invariant under reflective transformation derived by bilateral symmetry plane. Any pair of points on the surface of livestock defines a unique symmetry plane. Hence such a pair can be understood as one vote for this specific symmetry plane. By looking at all such pairs we can accumulate the votes and extract the symmetry plane. Only if pair of points located on (roughly) the same horizontal plane, do we have reason to believe that the corresponding symmetry is valid in the 3D shape C_* due to the perpendicularity between symmetry plane of livestock and ground plane. This observation will lead us to prune the set of all point pairs and avoid an exhaustive computation. More specifically, we start from creating a set of virtual planes $V = \{V_i \mid i = 0, 1, 2, \ldots\}$ by moving ground plane P_g along the direction of $\mathbf{n_g}$ with a distance interval δ. Here θ is maximum height of corresponding livestock species. Let $d(V_x, p_i)$ denote the euclidean distance from point p_i to plane V_x. Then we obtain intersection profiles between livestock C_* and those series of horizontal planes, find the largest profile defined as:

$$V = \arg\max_{V_j} \{p \mid d(V_j, p) \leqslant \frac{\theta}{2}, p \in C_*\},$$
$$L = \{p_i \mid d(V_*, p_i) \leqslant \frac{\theta}{2}, p_i \in C_*\}, \quad (1)$$

where L is the largest profile in terms of points number, θ is the distance between two virtual planes. Thus only points in L are considered as suitable candidates for bilateral symmetry relation, which avoids an exhaustive computation of $C_* \times L$ number of point pairs. Fig. 5 shows a visualization of the largest profile L that is passed to the next stage of bilateral symmetry plane detection.

PAIRING AND voting. Given the reduced set of point clouds L, we can now compute transformations for pairs of points in L. Similarly, only if pair of points located bilaterally, do we infer that the corresponding symmetry induced by the pairs of points is valid in the 3D shape C_* due to the bilateral symmetry fact. Thus we can make further optimization by constructing pairs of points located bilaterally. We start by choosing a set of one-to-many samples on L, which will be used for hypothesizing the existence of a group of specific bilateral symmetry. Let $K = \{k_i = (s_i, \{t_{ij}\}) \mid s_i \in L, t_{ij} \in L\}$ denote the one-to-many samples. For each pair of k_i, its first element s_i is selected randomly from L, while its second element is computed according to selected s_i by investigating the global frame of L. Specifically, we compute covariance matrix **Cov** as follows:

$$\bar{\mathbf{o}} = \frac{1}{N}\sum_{i=1}^{N} \vec{p}_i,$$
$$\mathbf{Cov} = \frac{1}{N}\sum_{i=1}^{N} (\vec{p}_i - \bar{\mathbf{o}})(\vec{p}_i - \bar{\mathbf{o}})^T,$$
$$\mathbf{Cov} \cdot \vec{v}_j = \lambda_j \cdot \vec{v}_j, \; j \in \{1, 2, 3\} \quad (2)$$

where N is the number of points of largest profile L, $\vec{p}_i$ represents the vector representation of point $p_i \in L$, $\bar{}$ denotes the 3D centroid of point clouds L, λ_j is the j-th eigenvalue of the covariance matrix while $\vec{v_j}$ is the j-th eigenvector. Notice that eigenvectors are sorted by corresponding eigenvalues largest to smallest. In other words, the first principle component represents the most variance and the last component the least. The principal directions define a global frame $(\vec{v_1}, \vec{v_2}, \vec{v_3})$, with origin located at point $\bar{}$. Based on the observation that anterior-posterior axis points in the direction of the most variance, dorsal–ventral axis points in the direction of the least variance. Let Π' denote the plane defined by normal vector $\vec{v_2}$ and point $\bar{}$. We observe that the plane Π' and the plane of reflection symmetry of L are almost overlapping. Let s_i' denote the reflected point of s_i with reflection plane Π'. Then we determine the second element $\{t_{ij}\}$ by using k-nearest neighbors of s_i'. This process is then repeated using the next random point in L until $N \times K$ number of one-to-many samples have been obtained. N is a user parameter which controls the complexity of the algorithm by limiting the search to loops of length N. Thus any pair of points (s_i, t_{ij}) defines a unique reflective symmetry, which provides our hypothetical symmetry samples and its corresponding hypothetical symmetry.

The pairing computed in the previous stage provides us with a hypothesis space. To extract correct bilateral symmetry we think of each pair in C_* as voting for a specific symmetry in the hypothesis space. Thus the symmetry plane of livestock will end up as the highest-vote-getting candidate in the hypothesis space. Specifically, for each pair in K we start from computing the corresponding hypothetical symmetry plane defined through a normal n_s and a scalar distance β_s of the plane from the origin. Each point p_i in C_* casts a vote for the hypothetical symmetry plane under two conditions: if its reflected point $p_i' = p_i - 2n_s(p_i^T n_s - \beta_s)$ is sufficiently close to a point t_j in C_*, and if it is on the plane. The former condition is implemented by testing whether $d_e(p_i' - t_j) \leqslant 3r$, where d_e is the Euclidean distance, t_j is determined by searching the single nearest neighbor of p_i' in the kd-tree of C_*. Thus this inner loop determines the number of votes of corresponding hypothetical symmetry plane. Let V_* denote the largest number of votes so far. The outer loop terminates when V_* stops growing, or when all pairs in K are considered. Eventually, a global peak is determined in the for the voting procedure. Fig. 6 shows a visualization of one-to-many samples

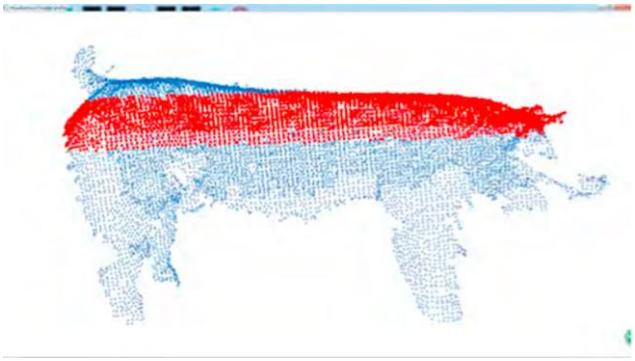

Fig. 5. The visualization of the largest profile L in red color that is the output of point pruning step. (For interpretation of the references to colour in this figure legend, the reader is referred to the web version of this article.)

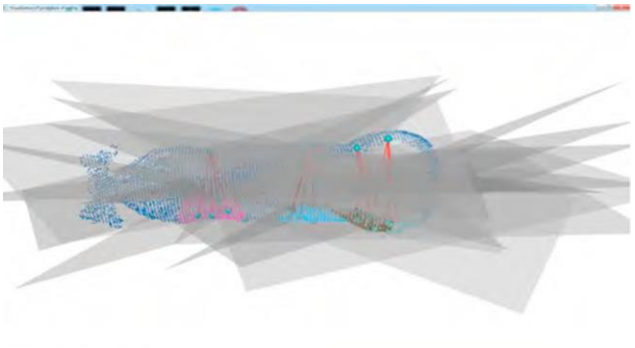

Fig. 6. Visualization of one-to-many samples in different colors and its corresponding hypothetical symmetry for some pairs of points (s_i, t_{ij}).

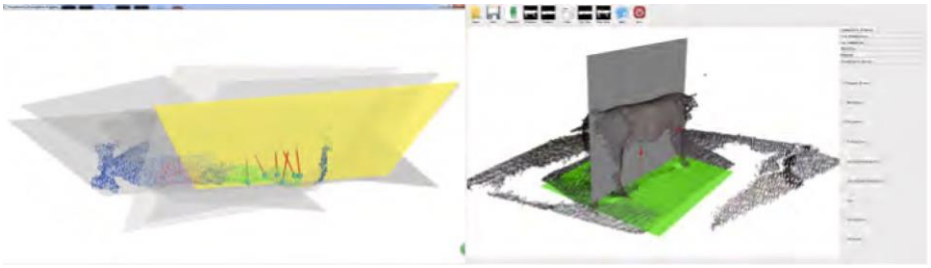

(a) Visualization of highest-vote-getting candidate plane with yellow color in the hypothesis space.

(b) Symmetry plane detected and its normal vector for the data of **Fig.1**

Fig. 7. Visualization of pairing and voting results.

voting space, the corresponding parameters n_s and β_s are used to define the estimated bilateral symmetry, as the yellow plane shown in Fig. 7a. Fig. 7b shows a visualization of symmetry plane detected and its normal vector for the data of Fig. 1.

2.2.4. FORWARD direction ESTIMATION

Similarly, there is no mathematical way to make sure that $\mathbf{n_s}$ points to the right side of livestock. Thus we can not define the Z-axis with $\mathbf{n_s}$ straightforwardly. Unlike the bilateral geometry of livestock, the top view contour shapes of front part of most livestock are more complex than its rear part due to the fact that livestock ears, snouts and horns are located on their front part. We exploit this characteristic to orient $\mathbf{n_s}$ towards right-side of livestock and determine the Z-axis by constructing one new application-specific geometric feature to discriminate between livestock front part and its rear part. Specifically, we begin by computing third axis using following equation:

$$\mathbf{n_x} \quad \mathbf{n_g} \quad \mathbf{n_s}, \tag{3}$$

where $\mathbf{n_x}$ is X-axis with undermined sign. To obtain top view contour shapes of livestock, we project each point of $\mathcal{C}$ onto the ground plane P_g. Then the same downsampling procedure used for input point clouds is applied on all points of projection to obtain new point clouds denoted by C_p. Additionally, splitting C_p in half along the line of symmetry which is perpendicular with $\mathbf{n_x}$ and belongs to minimum bounding rectangle of C_p, the resulting two 2D point clouds are denoted by C_{pi} with $i = \mathbf{1, 2}$. We apply the algorithm proposed in (Moreira and Santos, 2007) to extract the contours of C_{pi} with $k = \mathbf{8}$, which has proved to be a reasonable setting for all data we have tested. Here the only algorithm parameter k is used to control the smoothness of the final contour curve. For more details on how to set k we refer to (Moreira and Santos, 2007). Let H_{pi} denote the contour curve of C_{pi} respectively. In order to quantify the complexity of the top view shape contours, we explore the use of bending energy (van Vliet and Verbeek, 1998) as a shape parameter to describe and compare H_{pi} globally. Bending energy is a generalization of Bernoulli's "elastica" energy that measures the square of curvature integrated over the length of a given curve. The curvature induced by livestock ears, snouts and horns significantly increases the elastic energy, leading to classification rule that we can infer that the half side of C_{pi} with larger value, in terms of bending energy of H_{pi}, is the front of livestock. Thus we implement scale independent bending energy divided by the perimeter length of corresponding curve as follows. Let $H_{pi}(t) = (x(t), y(t))$ denote each 2D curve H_{pi}. The signed curvature and bending energy E_{pi} are computed via

$$\kappa(t) = \frac{\frac{dx}{dt}\frac{d^2y}{dt^2} - \frac{dy}{dt}\frac{d^2x}{dt^2}}{\left(\frac{dx}{dt}^2 + \frac{dy}{dt}^2\right)^{\frac{3}{2}}}$$

$$E_{pi} = \frac{1}{P_{pi}} \int_0^{dt} \kappa(t)dt \tag{4}$$

respectively. Where t is the parameter defined by using arc length curve parameterization, P_{pi} is the perimeter length of curve H_{pi}, $\kappa(t)$ is the curvature for point in terms of the parameter t.

Using results of bending energy of H_{pi}, it follows that we can determine that the half side of C_p with larger bending energy is the front part of livestock denoted by C_{pf}, as shown in Fig. 8a. The other half side of C_p is denoted by C_{pb}. Then we define one vector $\mathbf{v_f}$ to represent front direction of livestock using following equation:

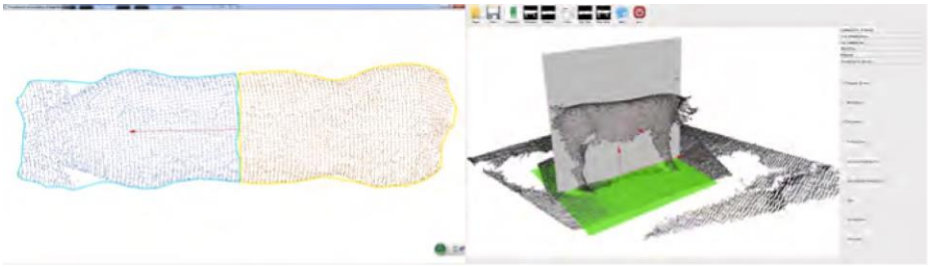

(a) Top view contour shapes of livestock front part C_{pf}, its back part C_{pb} and front direction vector $\mathbf{v_f}$.

(b) Visualization of final three axes estimated for the data of **Fig. 1**.

Fig. 8. Visualization of forward direction estimation and its final output.

$$\mathbf{v}_f = \mathbf{v}_{pf} - \mathbf{v}_{pb},$$
$$\mathbf{v}_{pf} = \frac{\sum_{i=1}^{N} p_i}{N}, p_i \in C_{pf}$$
$$\mathbf{v}_{pb} = \frac{\sum_{j=1}^{M} p_j}{M}, p_i \in C_{pb}, \quad (5)$$

where $\mathbf{v}_{pf}$ is the center of mass of C_{pf} with N points, $\mathbf{v}_{pb}$ is the center of mass of C_{pb} with M points. Finally, in order to make sure that the directions of vectors $\mathbf{n}_x$ and $\mathbf{n}_s$ can be used for X-axis, Z-axis respectively, their directions are reversed under condition:

$$\mathbf{v}_f \cdot \mathbf{n}_x \quad 0. \quad (6)$$

We thus obtain the final three principal axes for the canonical coordinate system. Fig. 8b shows a visualization of final three axes estimated for the data of Fig. 1. They are passed to the next stages of processing.

2.2.5. Pose normalization transformation

In this section, for the purpose of calculating pose normalization for livestock based on a 3D rigid transformation estimated from the three principal axes computed in the previous stages, we start by computing the center of mass of C_*, which is denoted by P_o, using last sub-equation of Eq. (5). Then two corresponded point sets $\{c_i\}$ and $\{o_i\}$, $\quad 1 \cdots 3$, are defined as follows. Let each element of $\{o_i\}$ be the coordinates in the canonical coordinate system and let each element of $\{c_i\}$ be the coordinates in the original coordinate system defined when capturing data. Without loss of generality, we will assume that $o_1 \quad [1\,0\,0], o_2 \quad [0\,1\,0], o_3 \quad [0\,0\,1]$ here. Then, $c_1 \quad P_o \quad \mathbf{n}_x, c_2 \quad P_o \quad \mathbf{n}_g$ and $c_3 \quad P_o \quad \mathbf{n}_s$ are computed.

Given the three pairs of corresponding points obtained above, such that they are related by:

$$o_i \quad \mathbf{R}_{co} c_i \quad \mathbf{T}_{co} \quad (7)$$

where $\mathbf{R}_{co}$ is a standard $3 \quad 3$ rotation matrix, $\mathbf{T}_{co}$ is a 3D translation vector. Thus $[\mathbf{R}_{co}, \mathbf{T}_{co}]$ defines the pose normalization transformation. Solving for this transformation that maps the set c_i onto o_i typically requires minimizing a least squares error criterion given by:

$$\Sigma = \sum_{i=1}^{3} \| o_i \quad \mathbf{R}_{co} c_i \quad \mathbf{T}_{co} \|^2 \quad (8)$$

Singular value decomposition (SVD) based method is employed to minimize Eq. (8). For complete derivations of this technique, the reader is invited to consult the paper(Eggert et al., 1997). Then the transformation estimated is applied on C_* so as to obtain the pose-normalized point clouds denoted by C_t. Fig. 9 shows a visualization of normalization result on the data of Fig. 1. All subsequent steps for body measurement are applied on C_t.

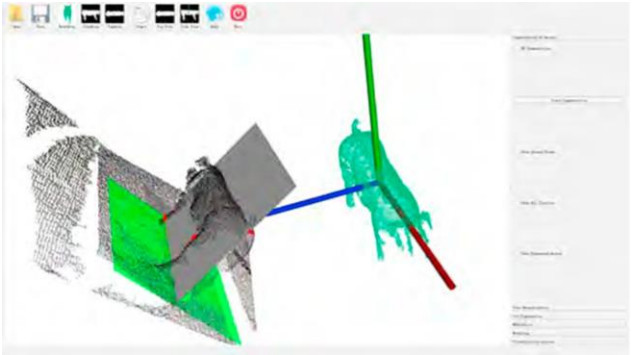

Fig. 9. Visualization of normalization result on the data of Fig. 1.

2.3. Livestock body measurement application and experimental data

Since the proposed algorithm reliably and automatically normalize livestock that in arbitrary pose, it is applicable to body measurements of multiple livestock species. To demonstrate the potential of the algorithm, we have implemented a livestock body measurement software framework that integrates the proposed approach as an alternative to *PCA* based pose normalization. In addition to avoiding manual interaction of setting forward direction of livestock, this improvement can make the software more robust to livestock head pose and data missing issues faced in paper(Guo et al., 2017). We refer readers to the paper (Guo et al., 2017) for more details about the software framework. Here we focus on showing how our new pose normalization algorithm can be helpful in measurement landmark detection so as to increase the degree of measuring automation in the following sections. As we all know, each livestock species has its own anatomical and morphometric particularity. Without loss of generality, here we only briefly present the detection procedure of body measurement landmarks for pigs.

2.3.1. Automatic detection of body measurement landmarks for pigs

The identification of landmarks that are well-defined and have anatomical meaning allows shape to be characterized in a manner that corresponds across subjects and that therefore provides the basis of subsequent statistical analysis. For the application of body measurements of pigs, detailed definitions of landmarks is provided by White et al. (2004) and this remains a standard reference. To localize those landmarks, we combine one dimensional signal obtained from the bilateral half of livestock point clouds and the intrinsic shape properties of corresponding landmarks. A visual diagram of automatic detection of body measurement landmarks for pigs is shown in Fig. 10. Specifically, we start from splitting the pose-normalized point clouds C_t in half resulting left half point cloud C_{tl} $\{p_i | p_i . z \leqslant 0\}$ and right half point cloud C_{tr} $\{p_i | p_i . z \geqslant 0\}$, where $p_i . z$ is z-coordinate of point p_i. Then for the left half point cloud C_{tl}, we construct a 1-D signal as $y \quad f(x)$ where x is the x-coordinate of point $p_i \in C_{tl}$, function value y is determined by the y-coordinate range of all points from C_{tl} which have an x-coordinate of x. To make this function suitable for numerical evaluation, discretization is performed by dividing the values of x into a small number of intervals, where each interval is mapped to a discrete. At the same time, the first derivative of the function f, $\frac{dy}{dx}$ is computed. Then peak detection of function $y \quad f(x)$ and steep slope of its corresponding first derivative function $\frac{dy}{dx}$ tell us that the x-coordinate of two left hooves. The same procedure is applied on right half point cloud. Thus we obtain the x-coordinate of position of four hooves, from which we can infer that the spatial relationships among the landmarks.

Let x_1, x_2, x_3, x_4 denote the x-coordinate of positions of front left, front right, rear left and rear right hooves respectively. For the two landmarks located at shoulder of pigs, we can define a volume of interest (*VOI*) by cropping one point cloud between two parallel planes which are defined by x_1 and x_2. Then the extreme points, min/max points in Z of the *VOI* are extracted, namely two landmarks located at shoulder of pigs. Similarly, the same procedure is employed for detection of the two landmarks located at pelvic limb of pigs. The position of landmark E is estimated by searching the maximum 3D points in Y of the point cloud C_t. The position for girth measurement is determined by translation of the geometric center of landmark A and B along the negative x-axis with a distance of μ. Where μ is an empirical parameter determined by the width of front leg. We thus obtain all landmarks for body measurements. See Fig. 11 for a visualization of all landmarks detected on the data of Fig. 1 and the corresponding body measurements in livestock application.

2.3.2. Experimental data

The first dataset is point clouds of live pigs in real world. Specifically, we used random selection to choose ten Landrace pigs with

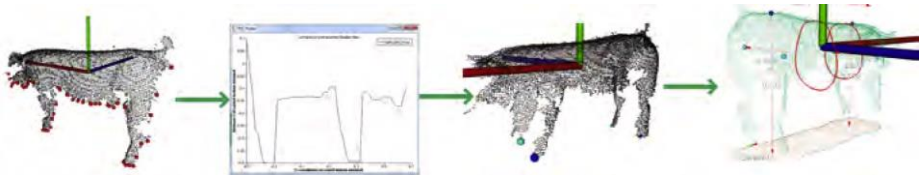

(a) Splitting the pose-normalized point clouds C_t in half.

(b) Constructing a 1-D signal as $y = f(x)$ and discretizing it.

(c) Peak detection in order to obtain the x-coordinate of position of four hooves.

(d) Landmarks location based on x-coordinate of position of four hooves and other geometric constraints.

Fig. 10. A visual diagram of automatic detection of body measurement landmarks for pigs.

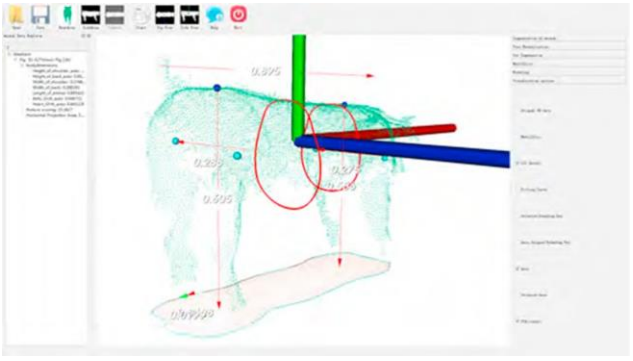

Fig. 11. All landmarks detected on the data of Fig. 1 and the corresponding body measurements in livestock application.

long bodies, short hair ranging in age from 130 to 220 days, from the ShangDong WeiHai swine-breeding center of DA BEI NONG GROUP to be scanned in our study. The heights of these animals were between 52 and 66 cm(cm), while their lengths varied from 80.5 to 104 cm(cm). Each subject of 10 live pigs was manually measured using the standard Lydtin stick in order to assess heights, widths and lengths while the circumference was evaluated through a tape meter. For each pig, live 3D point clouds sequences were captured by using the prototype system for animal 3D scanning (Guo et al., 2017), followed by selecting 15 point clouds of each pig with different posture from the sequences by applying the correct posture detection method in Guo et al. (2017). Thus a total of 150 point clouds of live pigs with constrained posture comprise our first data-set. During the data collection process, the target pig to be scanned is protected from direct sunlight. All scanned scene point clouds contained floor, farm facilities, and the pigs to be measured. Despite the point cloud quality changed slightly with distance, the effect of distance from the Xtion Pro sensor to the pigs is not investigated. All the scanning distance is from 0.8 to 1.6 m. The average point spacing of these point clouds r is set equal to 0.005 m. The second dataset is point clouds data of six livestock species created from synthetic dataset (Bing Yu, 2005), namely 3 pigs, 2 horses, 3 cows, 2 hippos, 2 rhinos, 2 water buffalo. This link (Bing Yu, 2005) provides a repository of 3D models for evaluating shape analysis algorithms. The motivation is to promote the use of standardized data sets and evaluation methods for research in matching, classification, clustering, and recognition of 3D models. Researchers are encouraged to use these resources to produce comparisons of competing algorithms in publications. Comparatively speaking, those 3d shapes are smooth and have genus zero. It is worth noting that synthetic dataset only have symmetric posture of 3D model animal for testing, except for horses. Due to inconsistent size of each model, we normalized model size by scaling its bounding box to avoid twisting parameters used for pose normalization. Additionally, those 3D models are 3D mesh model without ground plane. In order to satisfy the requirements described in Section 2.1, Meshlab (Cignoni et al., 2008) was used to add a virtual ground plane and convert the mesh into point cloud using uniform sampling at the resolution of r **0.005**.

3. Results and discussion

We present qualitative and quantitative results on both real world point clouds and synthetic 3D scenes. All 3D datasets are processed with constant parameter values. Specifically, the octree leaf size for down-sampling d_r is set equal to $\mathbf{3}r$, where r is point cloud resolution, distance interval θ for point pruning is $\mathbf{0}r$, the number of one-to-many samples N for pairing and voting is 20, the iterations of RANSAC for ground plane detection is 10,000 while the tolerance threshold ε is $\mathbf{3}r$. Evaluating alignment methods directly is difficult as, in the best case, the evaluation may be based on a subjective ground truth alignment that a human operator performed on a dataset. However, since pose normalization tasks are primarily used as a preprocessing procedure in several graphics applications, including 3D object retrieval and biometrics, it is possible to evaluate the performance of an alignment method through the results of its application(Sfikas et al., 2014). Therefore, the experiments presented in this section are designed to evaluate the accuracy of our approaches for pose normalization of livestock and to analyze its application in a 3D point clouds analysis software for the task of landmark detection and body measurement of livestock. The following subsections will elaborate on the validation for each experiment respectively.

3.1. *Livestock pose* NORMALIZATION

We compare our pose normalization method and baselines with the following two method: (1) the first one is Principal Component Analysis (*PCA*) which is the best-known baseline pose normalization method (Vranic et al., 2001), available in the Point Cloud Library (Rusu and Cousins, 2011). (2) The second one is a modified principal component analysis (*MPCA*) algorithm and designed only for normalization of point clouds of pigs (Wang et al., 2017). In the following, the proposed pose normalization approach will be denoted as *SPNA*. Let θ_s^x, θ_s^y, θ_s^z be values of angles in degrees formed by two vectors of corresponding axes between ground truth and pose normalization results of *SPNA*. Then the errors of *SPNA* is given by $SPNA_e$ θ_s^{x2} θ_s^{y2} θ_s^{z2}. Similarly, PCA_e and *MPCA* $_e$ can be defined as the errors of the corresponding method. Note that in order to avoid that PCA_e contains error component leading

Table 1
Results of comparison between pose normalization approaches for the first dataset. *PCA* stands for Principal Component Analysis which is the best-known baseline pose normalization method (Vranic et al., 2001). *MPCA* stands for modified principal component analysis algorithm in paper (Wang et al., 2017). *SPNA* stands for our proposed pose normalization approach. Column Mean, Std represent average errors ($SPNA_e$, PCA_e and $MPCA_e$ respectively) and its standard deviation for corresponding method on the 150 point clouds of live pigs, FDD (Forward direction determination) represents whether or not the corresponding method can determine the forward direction of livestock while SLS (Supported livestock species) represents which of livestock species can be supported by corresponding method.

Method	Mean error	Std	FDD	SLS
SPNA	12.4	2.2	Yes	Pig
MPCA	22.6	2.2	No	
PCA	55.2	4.6	No	

by the wrong direction of axis or wrong corresponding axis, we use the smaller of the angles formed by the all possible combinations of axes. The ground truth of pose normalization was obtained manually on the test datasets.

Results on REAL world DATA (pigs). The dataset in which we have validated our pose normalization method on was point clouds of live pigs. We present quantitative results in Table 1. A single factor analysis of variance (ANOVA) was performed. Each of groups represents errors of corresponding methods consisting of 150 samples. The null hypothesis is that the means of the errors from different methods are equal. The results show that critical value Fc **(3.02)** F **(4801.63)**. So the null hypothesis can be rejected. Note also that P_{value} α which is set by default to 0.05. Therefore there is sufficient difference in the errors recorded by those three methods. Our method outperform *PCA* significantly, and are only slightly superior to *MPCA* the state-of-the-art pose normalization method for pigs (Wang et al., 2017). As the Fig. 12 shows, with real world data, the errors obtained with the *PCA* method mainly caused by two reasons. The first one is that non-bilateral symmetric posture of livestock lead to X axis of *CCS* pointing left or right, such as one animal standing with its head tilted aside. The second one is that the second principle component of *PCA* normally is not perpendicular to the ground plane due to different species or conditions of data noise. Thus our method has several advantages over *PCA* on these data since it exploits information of ground plane and symmetric plane from the point clouds and makes some assumptions about the input 3D data. While *MPCA* only explores the normal vector of ground plane as a geometric hint to adjust the output of *PCA*. As shown in Fig. 12, our approach can handle real world data with non symmetric missing parts or with its head aside.

Results on synthetic DATA (pigs, cows, hippos, horses, rhinos, WATER BUFFALO). Our pose normalization method was also applied to a second dataset built with point clouds data of synthetic dataset. Figs. 13 and 15 shows representative results for each species. This experiment involved a challenging object, namely the horse shown in Fig. 13. This object possesses four moving legs and its head tilted aside. However, its major body part is symmetrical which can lead to positive results owing to our pairing-voting scheme. Here we only provided qualitative results on the second dataset since we didn't have enough samples for quantitative evaluation. It is worth pointing out that our method has potential for generalizing well across livestock species on account of our novel algorithms of symmetry detection and forward direction determination.

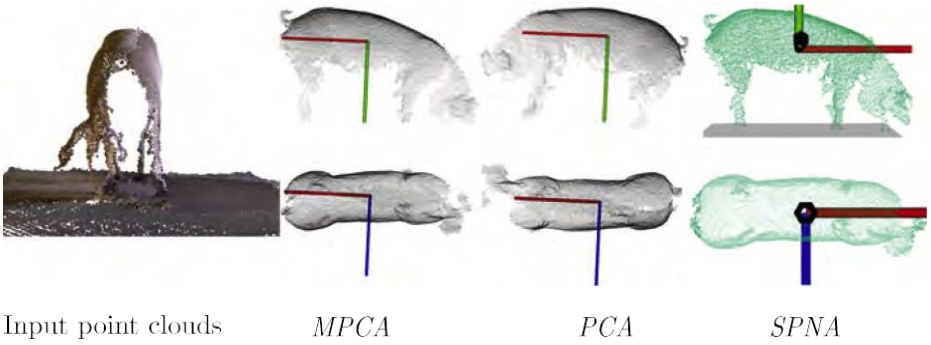

Fig. 12. Examples of pose normalization results using different approaches presenting the data with non symmetric missing parts or with its head aside.

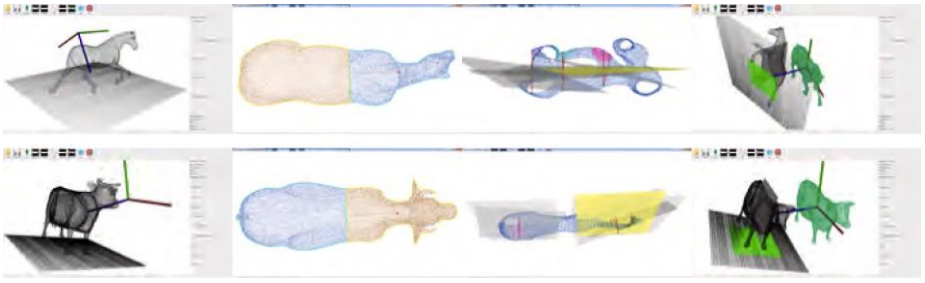

Fig. 13. Visualization of representative results on synthetic data.

Table 2
Comparisons between the mean value of live pigs body measurements measured manually and using LSSA_CAU integrated with different pose normalization method. *With_PCA* and *With_SPNA* stand for LSSA_CAU integrated with *PCA* and *SPNA* for its pose normalization procedure. Column Mean, Std represent average percent errors and its standard deviation for corresponding method on the 150 point clouds of live pigs, SA (Support automation) represents whether or not the corresponding method can take measurements automatically while BM (Body measurements) represents various morphometric traits.

Method	Mean(%)	Std	SA	BM
With_PCA	2.4	5.3	No	Body length
With_SPNA	5.6	4.9	Yes	
With_PCA	5.8	4.8	No	Withers width
With_SPNA	6.8	5.0	Yes	
With_PCA	7.4	5.1	No	Withers height
With_SPNA	8.1	6.8	Yes	
With_PCA	4.7	8.5	No	Hip width
With_SPNA	5.6	5.2	Yes	
With_PCA	4.8	2.8	No	Hip height
With_SPNA	3.0	3.4	Yes	

3.2. APPLICATIONS

This section are minded to evaluate influence of our pose normalization method on the task of landmark detection and body measurement of livestock. The dataset, on which the experiments of landmark detection and body measurement were conducted, is the 150 point clouds of live pigs mentioned above.

3.2.1. Results of LANDMARK detection

Our experimental evaluation of landmark detection is based on two quantitative measures: localization displacement (LD), detection rates (DR). The localization displacement (LD) is estimated as the 3D Euclidean distance between the ground truth position and the position obtained through our detection approach. The ground truth position to each landmark was manually labeled. Detection rates were obtained by counting the percentage of detected landmarks whose localization displacement was below the threshold. Here we set the threshold of 0.05 m for satisfying body measurement application. The mean error and the standard deviation were computed considering the localization displacement between the ground truth and our automatic detection output. Average errors and its standard deviation for localization displacement on all landmarks are **20.4 (mm)** and **8.2 (mm)** respectively, while detection rates is **88%**. Some results of the landmark detection are shown in Fig. 16. Notice that our landmark detection algorithm is a very naive method owing to there is a clear prior knowledge about posture of the livestock obtained from our pose normalization scheme. However, our landmark detection method can not estimate the locations of missing landmarks in raw point clouds data. We argue that there are more robust landmark detection algorithms. One could employ shape based landmark detection (Gilani et al., 2015) to handle the landmarks missing issue, but we leave this as future work. Then, landmarks were employed to automatically obtain body measurement of livestock.

3.2.2. Results of body MEASUREMENT

In order to evaluate the performance of pose normalization method through the results of body measurement application, we have chosen the LSSA_CAU, state-of-the-art 3D livestock body measurement software (Guo et al., 2017). The proposed method replaces the *PCA* pose normalization method in the existing hybrid scheme. Additionally, we implement the integration of our landmark detection algorithm into LSSA_CAU. Each subject of live pigs was manually measured using the standard Lydtin stick in order to assess heights, widths and lengths

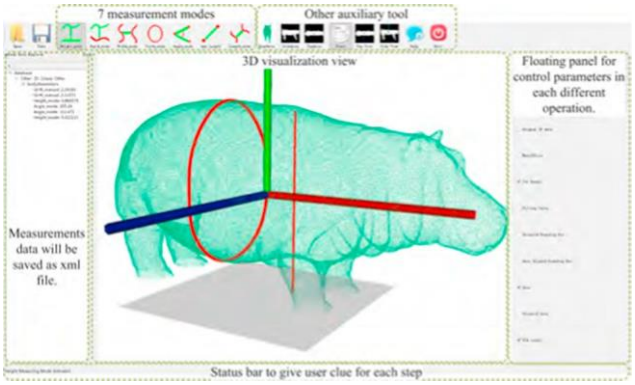

Fig. 14. *SPNA* based livestock body measurement software user interface.

while the circumference was evaluated through a tape meter. We performed the corresponding body measurements on point clouds data of these live pigs by using the LSSA_CAU with different pose normalization method. Note that *PCA* based system only support taking measurements by user interaction while *SPNA* based system can take measurements automatically. Table 2 shows the results of body measurements using different configuration.

Error percentage achieved demonstrated that all of methods can reach levels of measurement accuracy comparable to those obtained by traditional measuring instruments. It should be noted that more accuracy can be obtained by using more advanced 3D scanning system. In addition to avoiding the input of forward direction and time consuming landmark picking procedure, our *SPNA* pose normalization based system presents a slightly worse precision in comparison to *PCA* based system. The combination of *SPNA* and our landmark detection procedure would provide a automatic solution for pig body measurement. Fig. 14 shows the software user interface with Hippo. It is worth pointing out that, comparing with current body measurement related reports (Viazzi et al., 2014; Tasdemir et al., 2011), most of traits can be measured easily with less user interaction in this framework. Besides, our pose normalization can handle more livestock species.

4. Conclusions

A novel pose normalization method for 3D point clouds of livestock with similar forms of cows or pigs based on its bilateral symmetry properties and geometric characteristics, is proposed. Such approach can handle various livestock species, provided that the input data satisfy requirements of the algorithm. We have shown results on real world and synthetic datasets including comparisons with most well known method *PCA* and state-of-the-art pose normalization method *MPCA* for pigs that demonstrate that our method is competitive. *SPNA* is successfully integrated into a 3D livestock body measurement system as a pose normalization preprocessing step. Furthermore, the proposed method is able to improve the degree of measuring automation for livestock body measurement system which can be used for health monitoring, weighing and so on. However, some species with long tails may lead to incorrect output in the forward direction estimation of our approach. Thus real world livestock species other than pigs need to be tested and will be next priority for researchers. The assumption that only one animal exists in the 3D scene does not hold in some cases when we're considering commercial and industrial usage. Given that multiple animals can be an issue to segmentation of our system this limitation should be addressed in future.

Acknowledgment

The authors wish to thank everyone who participated in the software assessment, both taking 3D data and manually measuring traits.

Thanks to Shang-Dong WeiHai swine-breeding center of DA BEI NONG GROUP they provide us materials for experiment. We also acknowledge the comments of the referees, which have significantly improved the text. This work was supported by National Natural Science Foundation of China [Grant Nos. 41601491]; The Fundamental Research Funds for the Central Universities [Grant Nos. 2018QC080, 2018TY002].

Appendix A. Additional materials

See Table 3.
See Figs. 15 and 16.

Table 3
All of the abbreviations.

Abbreviations	Full names or meanings
PLF	Precision livestock farming
CCS	Canonical coordinate system
SPNA	Our proposed pose normalization approach
MPCA	Modified principal component analysis algorithm in paper(Wang et al., 2017)
FDD	Forward direction determination
SLS	Supported livestock species
PCA	Principal component analysis

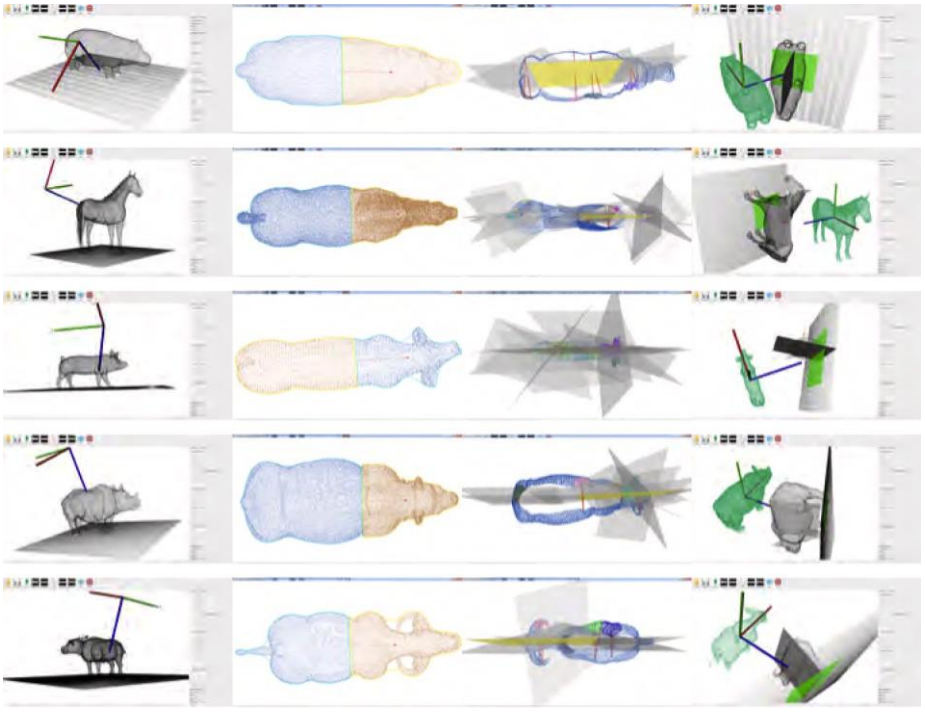

Input livestock point clouds. Forward direction estimation. Bilateral symmetry plane detection of livestock. Pose normalized livestock.

Fig. 15. Visualization of representative results on synthetic data.

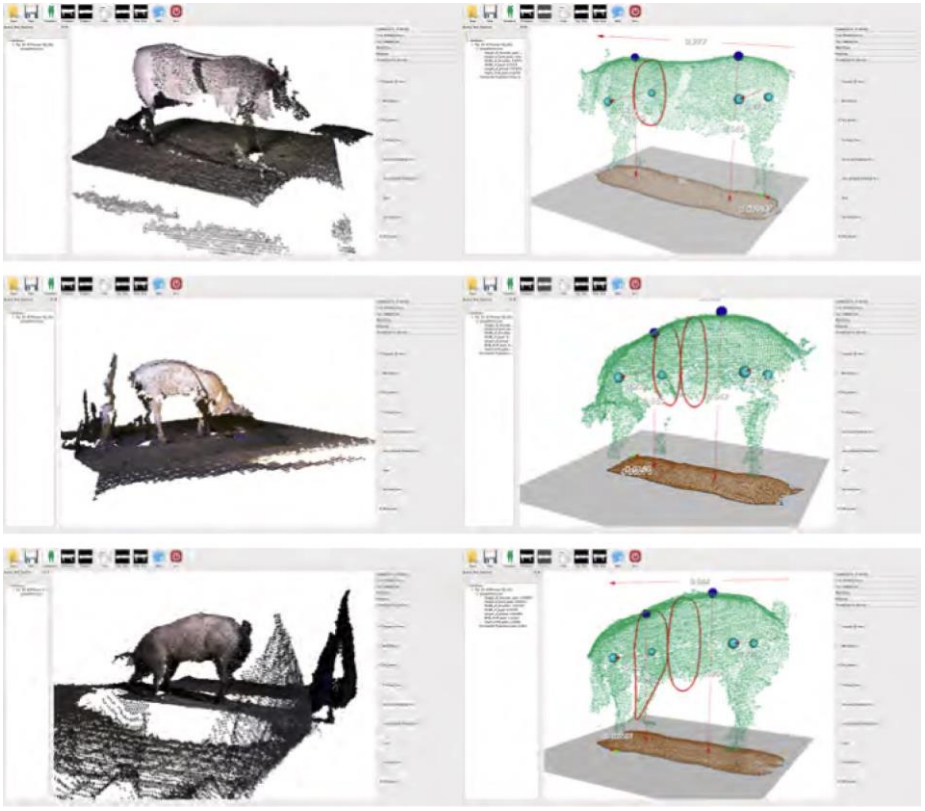

Input livestock point clouds. Landmarks detection output.

Fig. 16. Visualization of landmarks detection results on real world data.

Appendix B. Supplementary material

Supplementary data associated with this article can be found, in the online version, at https://doi.org/10.1016/j.compag.2019.03.010.

References

Savin, T., Kurpios, N.A., Shyer, A.E., Florescu, P., Liang, H., Mahadevan, L., Tabin, C.J., 2011. On the growth and form of the gut. Nature 476 (7358), 57–62. https://doi.org/10.1038/nature10277.

Klingenberg, C.P., 2010. Evolution and development of shape: integrating quantitative approaches. Nat. Rev. Genet. 11 (9), 623–635. https://doi.org/10.1038/nrg2829.

Azzaro, G., Caccamo, M., Ferguson, J.D., Battiato, S., Farinella, G.M., Guarnera, G.C., Puglisi, G., Petriglieri, R., Licitra, G., 2011. Objective estimation of body condition score by modeling cow body shape from digital images. J. Dairy Sci. 94 (4), 2126–2137. https://doi.org/10.3168/jds.2010-3467.

Tasdemir, S., Urkmez, A., Inal, S., 2011. Determination of body measurements on the Holstein cows using digital image analysis and estimation of live weight with regression analysis. Compute. Electron. Agric. 76 (2), 189–197. https://doi.org/10.1016/j.compag.2011.02.001.

Kuzuhara, Y., Kawamura, K., Yoshitoshi, R., Tamaki, T., Sugai, S., Ikegami, M., Kurokawa, Y., Obitsu, T., Okita, M., Sugino, T., Yasuda, T., 2015. A preliminarily study for predicting body weight and milk properties in lactating Holstein cows using a three-dimensional camera system. Comput. Electron. Agric. 111, 186–193. https://doi.org/10.1016/j.compag.2014.12.020.

Brandl, N., Jorgensen, E., 1996. Determination of live weight of pigs from dimensions measured using image analysis. Comput. Electron. Agric. 15 (1), 57–72. https://doi.org/10.1016/0168-1699(96)00003-8.

Marchant, J., Schofield, C., White, R., 1999. Pig growth and conformation monitoring using image analysis. Anim. Sci. 68 (1), 141–150.

Wongsriworaphon, A., Arnonkijpanich, B., Pathumnakul, S., 2015. An approach based on digital image analysis to estimate the live weights of pigs in farm environments. Comput. Electron. Agric. 115, 26–33. https://doi.org/10.1016/j.compag.2015.05.004.

Yilmaz, O., Cemal, I., Karaca, O., 2013. Estimation of mature live weight using some body measurements in Karya sheep. Trop. Anim. Health Prod. 45 (2), 397–403. https://doi.org/10.1007/s11250-012-0229-7.

Menesatti, P., Costa, C., Antonucci, F., Steri, R., Pallottino, F., Catillo, G., 2014. A low-cost stereovision system to estimate size and weight of live sheep. Comput. Electron. Agric. 103, 33–38. https://doi.org/10.1016/j.compag.2014.01.018.

Pallottino, F., Steri, R., Menesatti, P., Antonucci, F., Costa, C., Figorilli, S., Catillo, G., 2015. Comparison between manual and stereovision body traits measurements of Lipizzan horses. Comput. Electron. Agric. 118, 408–413. https://doi.org/10.1016/j.compag.2015.09.019.

Salau, J., Haas, J.H., Junge, W., Thaller, G., 2017. A multi-kinect cow scanning system: calculating linear traits from manually marked recordings of holstein-friesian dairy cows. Biosyst. Eng. 157 (Supplement C), 92–98. https://doi.org/10.1016/j.biosystemseng.2017.03.001.

Mortensen, A.K., Lisouski, P., Ahrendt, P., 2016. Weight prediction of broiler chickens using 3d computer vision. Comput. Electron. Agric. 123, 319–326. https://doi.org/10.1016/j.compag.2016.03.011.

Wu, J., Tillett, R., McFarlane, N., Ju, X., Siebert, J., Schofield, P., 2004. Extracting the three-dimensional shape of live pigs using stereo photogrammetry. Comput. Electron. Agric. 44 (3), 203–222. https://doi.org/10.1016/j.compag.2004.05.003.

Lichti, D.D., Qi, X., Ahmed, T., 2012. Range camera self-calibration with scattering compensation. ISPRS J. Photogram. Remote Sens. 74 (Supplement C), 101–109. https://doi.org/10.1016/j.isprsjprs.2012.09.008. http://www.sciencedirect.com/science/article/pii/S0924271612001773 .

Weber, A., Salau, J., Haas, J.H., Junge, W., Bauer, U., Harms, J., Suhr, O., Schonrock, K., Rothfuss, H., Bieletzki, S., Thaller, G., 2014. Estimation of backfat thickness using extracted traits from an automatic 3D optical system in lactating Holstein-Friesian cows. Livestock Sci. 165, 129–137. https://doi.org/10.1016/j.livsci.2014.03.022.

Pezzuolo, A., Guarino, M., Sartori, L., Marinello, F., 2018. A feasibility study on the use of a structured light depth-camera for three-dimensional body measurements of dairy cows in free-stall barns. Sensors 18 (2), 673. https://doi.org/10.3390/s18020673.

Song, X., Bokkers, E.A.M., van der Tol, P.P.J., Koerkamp, P.W.G.G., van Mourik, S., 2018. Automated body weight prediction of dairy cows using 3-dimensional vision. J. Dairy Sci. 101 (5), 4448–4459. https://doi.org/10.3168/jds.2017-13094.

Kawasue, K., Ikeda, T., Tokunaga, T., Harada, H., 2013. Three-dimensional shape measurement system for black cattle using KINECT sensor. Int. J. Circ. Syst. Signal Process. 7 (4), 222–230.

Viazzi, S., Bahr, C., Van Hertem, T., Schlageter-Tello, A., Romanini, C.E.B., Halachmi, I., Lokhorst, C., Berckmans, D., 2014. Comparison of a three-dimensional and two-dimensional camera system for automated measurement of back posture in dairy cows.

Comput. Electron. Agric. 100, 139–147. https://doi.org/10.1016/j.compag.2013.11.005.
Guo, H., Wang, K., Su, W., Zhu, D.H., Liu, W.L., Xing, C., Chen, Z.R., 2017. 3d scanning of live pigs system and its application in body measurements. ISPRS – Int. Archiv. Photogram. Remote Sens. Spat. Inform. Sci. XLII-2/W7, 211–217. https://doi.org/10.5194/isprs-archives-XLII-2-W7-211-2017.
Pezzuolo, A., Guarino, M., Sartori, L., Gonzlez, L.A., Marinello, F., 2018. On-barn pig weight estimation based on body measurements by a Kinect v1 depth camera. Comput. Electron. Agric. 148, 29–36. https://doi.org/10.1016/j.compag.2018.03.003.
Kawasue, K., Khin, W., 2017. Black cattle body shape and temperature measurement using thermography and KINECT sensor. Artificial Life Robotics 22 (4), 464–470. https://doi.org/10.1007/s10015-017-0373-2.
Salau, J., Haas, J.H., Junge, W., Thaller, G., 2016. Extrinsic calibration of a multi-Kinect camera scanning passage for measuring functional traits in dairy cows. Biosyst. Eng. 151 (Supplement C), 409–424. https://doi.org/10.1016/j.biosystemseng.2016.10.008.
Salau, J., Haas, J.H., Junge, W., Thaller, G., 2017. Automated calculation of udder depth and rear leg angle in holstein-friesian cows using a multi-kinect cow scanning system. Biosyst. Eng. 160 (Supplement C), 154–169. https://doi.org/10.1016/j.biosystemseng.2017.06.006.
Vranic, D., Saupe, D., Richter, J., 2001.Tools for 3D-object retrieval: Karhunen-Loeve transform and spherical harmonics. In: Dugelay, J.L., Rose, K., (Eds.), 2001 IEEE Fourth Workshop on Multimedia Signal Processing. IEEE Signal Process Soc, Multimedia Signal Process Tech Comm; Cegetel; Hitachi; Texas Instruments; Inst Eurecom; Telecom Valley Assoc, 2001, pp. 293–298, 4th IEEE Workshop on Multimedia Signal Processing (MMSP 01), CANNES, FRANCE, OCT 03-05, 2001. doi: 10.1109/MMSP.2001.962749.
Chen, D., Tian, X., Shen, Y., Ming, O., 2003. On visual similarity based 3D model retrieval. Comput. Graph. Forum 22 (3, SI), 223–232. https://doi.org/10.1111/1467-8659.00669. 24th Annual Conference of the European-Association-for-Computer-Graphics (EUROGRAPHICS 2003), GRANADA, SPAIN, SEP 01-06, 2003.
Papadakis, P., Pratikakis, I., Perantonis, S., Theoharis, T., 2007. Efficient 3D shape matching and retrieval using a concrete radialized spherical projection representation. Pattern Recogn. 40 (9), 2437–2452. https://doi.org/10.1016/j.patcog.2006.12.026.
Guo, H., Ma, X., Ma, Q., Wang, K., Su, W., Zhu, D., 2017. LSSA-CAU: An interactive 3d point clouds analysis software for body measurement of livestock with similar forms of cows or pigs. Comput. Electron. Agric. 138 (Supplement C), 60–68. https://doi.org/10.1016/j.compag.2017.04.014. http://www.sciencedirect.com/science/article/pii/S0168169917301746 .
Bevilacqua, V., Andriani, F., Mastronardi, G., 2009. 3D head pose normalization with face geometry analysis, genetic algorithms and PCA. J. Circ. Syst. Comput. 18 (8), 1425–1439. https://doi.org/10.1142/S0218126609005769.
Sfikas, K., Theoharis, T., Pratikakis, I., 2011. ROSy+: 3d object pose normalization based on PCA and reflective object symmetry with application in 3D object retrieval. Int. J. Comput. Vis. 91 (3), 262–279. https://doi.org/10.1007/s11263-010-0395-x.
Sfikas, K., Theoharis, T., Pratikakis, I., 2014. Pose normalization of 3D models via reflective symmetry on panoramic views. Vis. Comput. 30 (11), 1261–1274. https://doi.org/10.1007/s00371-014-0935-4.
Hejrati, M., Ramanan, D., 2016. Categorizing cubes: revisiting pose normalization. In: 2016 IEEE Winter Conference on Applications of Computer Vision (WACV), 2016 IEEE Winter Conference on Applications of Computer Vision (WACV), pp. 1–9.
Zhang, M., Zhang, L., Mathiopoulos, P.T., Ding, Y., Wang, H., 2013. Perception-based shape retrieval for 3D building models. ISPRS J. Photogramm. Remote Sens. 75 (Supplement C), 76–91. https://doi.org/10.1016/j.isprsjprs.2012.10.001. http://www.sciencedirect.com/science/article/pii/S0924271612001840 .
Farrugia, T., Barbarar, J., 2015. Pose Normalisation for 3D Vehicles. Springer International Publishing, Cham. https://doi.org/10.1007/978-3-319-23192-1_20.
Wang, K., Guo, H., Liu, W., Ma, Q., Su, W., Zhu, D.H., 2017. Extraction method of pig body size measurement points based on rotation normalization of point cloud. Trans. Chinese Soc. Agric. Eng. 33, 253–259.
G. Hao, Point clouds processing software for livestock body measurement (2017). URL https://github.com/LiveStockShapeAnalysis.
Schnabel, R., Wahl, R., Klein, R., 2007. Efficient RANSAC for point-cloud shape detection. Comput. Graph. Forum 26 (2), 214–226. https://doi.org/10.1111/j.1467-8659.2007.01016.x.
Mitra, N.J., Guibas, L.J., Pauly, M., 2006. Partial and approximate symmetry detection for 3D geometry. ACM Trans. Graph. 25 (3), 560–568. https://doi.org/10.1145/1141911.1141924.
Moreira, A.J.C., Santos, M.Y., 2007. Concave hull: a k-nearest neighbours approach for the computation of the region occupied by a set of points. In: GRAPP.
van Vliet, L.J., Verbeek, P.W., 1998. Curvature and bending energy in digitized 2D and 3D images.
Eggert, D., Lorusso, A., Fischer, R., 1997. Estimating 3-D rigid body transformations: a comparison of four major algorithms. Mach. Vis. Appl. 9 (5-6), 272–290. https://doi.org/10.1007/s001380050048.
White, R.P., Schofield, C.P., Green, D.M., Parsons, D.J., Whittemore, C.T., 2004. The effectiveness of a visual image analysis (via) system for monitoring the performance of growing/finishing pigs. Anim. Sci. 78 (3), 409–418. https://doi.org/10.1017/S1357729800058811.
C. Bing Yu, 3d models (2005). URL http://www.cmlab.csie.ntu.edu.tw/robin/courses/cg03/model/.
Cignoni, P., Callieri, M., Corsini, M., Dellepiane, M., Ganovelli, F., Ranzuglia, G., 2008. MeshLab: an open-source mesh processing tool. In: Scarano, V., Chiara, R.D., Erra, U. (Eds.), Eurographics Italian Chapter Conference. The Eurographics Association. https://doi.org/10.2312/LocalChapterEvents/ItalChap/ItalianChapConf2008/129-136.
Rusu, RB, Cousins, S, 2011. 3d is here: Point cloud library (PCL).
Gilani, S.Z., Shafait, F., Mian, A., 2015. Shape-based automatic detection of a large number of 3d facial landmarks. In: 2015 IEEE Conference on Computer Vision and Pattern Recognition (CVPR), 2015, pp. 4639–4648. doi: https://doi.org/10.1109/CVPR.2015.7299095.